Solar Energy Materials & Solar Cells 236 (2022) 111534

Contents lists available at ScienceDirect

Solar Energy Materials and Solar Cells

journal homepage: www.elsevier.com/locate/solmat

Modeling parasitic absorption in silicon solar cells with a near-surface absorption parameter

Andreas Fell [a,*], Johannes Greulich [a], Frank Feldmann [a,c], Christoph Messmer [a,b], Jonas Schön [a,b], Martin Bivour [a], Martin C. Schubert [a], Stefan W. Glunz [a,b]

[a] Fraunhofer Institute for Solar Energy Systems (ISE), Heidenhofstrasse 2, 79110, Freiburg, Germany
[b] Department of Sustainable Systems Engineering, Albert Ludwig University of Freiburg, Georges-Köhler-Allee 103, D-79110, Freiburg, Germany
[c] Now with Solarlab Aiko Europe GmbH, Berliner Allee 29, 79110, Freiburg, Germany

ARTICLE INFO

Keywords:
Silicon solar cell
Parasitic absorption
Skin
Free carrier absorption
FCA
Poly-silicon
TCO
Passivating contacts
Light trapping
Modeling
TOPCon
Appp
Optics

ABSTRACT

One drawback of passivating contacts in crystalline silicon solar cells is the current loss due to parasitic absorption within the involved material layers. When employed on an illuminated side of the cell, the full spectrum of the incident light will be partly absorbed before reaching the silicon bulk. Additionally, near-infrared (NIR) absorption can substantially reduce the cell's NIR spectral response (SR) also when employed on the non-illuminated side. As those losses are hard to measure directly, optical modeling is crucial for their quantification. This paper presents an extension to an analytical light-trapping model to account for parasitic absorption in the near-surface region via a new parameter A_{ppp} (absorbed fraction per perpendicular pass). We test the model by analyzing i) reflectance measurements on samples with varying doping profiles, ii) SR measurements on TOPCon solar cells with varying back-side poly-silicon layers, and iii) SR measurements of a bifacial silicon heterojunction cell. We show that the model can well be calibrated by fitting a single value for A_{ppp} to reflectance measurements. This enables a quantification of the parasitic absorption loss without requiring knowledge of all layer's optical properties. The model also is able to predict parasitic absorption in TOPCon cells when knowing the thickness and doping density of the poly-Si layer. Having proven the usefulness of A_{ppp} to represent parasitic absorption as a single-valued quantity, we suggest A_{ppp} as a third figure of merit for the quality of a passivating contact, next to the recombination parameter J_{0c} and the contact resistivity ρ_c.

1. Introduction

The main purpose of a passivating contact in a silicon solar cell is to reduce recombination losses at the metallized regions, quantified by the recombination parameter J_{0c}. At the same time the contact resistivity ρ_c must be ensured to be small, and, if applied on a side with metal fingers, a low sheet resistance R_{sheet} is required to support lateral current transport. In particular the two quantities J_{0c} and ρ_c have been very successful figures of merit in judging and comparing the quality of different passivating contact technologies, as they can be directly applied within silicon solar cell modeling, see e.g. Ref. [1]. Next to requiring the balancing of those electrical properties, passivating contacts typically show substantial optical losses due to parasitic absorption, which needs to be taken into account when quantifying the influence on solar cell performance [2]. However, no figure of merit exists yet to easily quantify and compare the optical quality of passivating contacts. Often the term *transparency* is used to denote parasitic absorption, which however is a spectral property and does not account for the increased parasitic absorption in the near-infrared (NIR) due to multiple internal reflections, i.e. the light-trapping losses. Instead, detailed optical modeling of a particular cell design including the detailed optical properties of the passivating contact layers has to be performed, usually via ray tracing [2–6].

The optical modeling in this work denotes a passivating contact as a skin on the crystalline silicon (c-Si) bulk [7], where the skin comprises a thin near-surface c-Si region and further material layers. Parasitic absorption in the near-surface region of the c-Si absorber happens via free-carrier absorption (FCA) [8], which can be significant for typical doping profiles. For a thin oxide plus poly-Si layer passivating contact, like e.g. TOPCon [9], the total absorption in the poly-Si layer constitutes a parasitic absorption loss. For the silicon heterojunction (SHJ) technology, parasitic absorption takes place in the amorphous silicon (a-Si)

* Corresponding author.
E-mail address: andreas.fell@ise.fraunhofer.de (A. Fell).

https://doi.org/10.1016/j.solmat.2021.111534
Received 7 May 2021; Received in revised form 23 November 2021; Accepted 1 December 2021
Available online 6 December 2021

layers, as well as in the transparent conductive oxide (TCO) layer. Notably, the band-to-band absorption in the poly-Si and a-Si layers is not fully lost as a (typically small) fraction might be collected and still contribute to the generated current density [10]. The parasitic absorption of a skin should therefore be more precisely considered as the non-collected fraction of the total absorption in the skin. This electrical effect is however not considered in this work.

For understanding and modeling solar cell optics it is useful to distinguish *external* and *internal* optics, see Fig. 1: *external* optics means the optical characteristics of a skin when externally illuminated, i.e. external reflection R_{ext} and parasitic absorption A_{ext}, which both determine the external transmission T_{ext} being the fraction of incident photons available for absorption in the bulk; *internal* optics mean the cell's light-trapping properties, which is relevant only for not very strongly absorbing NIR wavelengths, typically between 900 nm and 1200 nm. When a passivating contact skin is placed on an illuminated side, the external absorption losses are usually substantial for the short wavelengths, i.e. dominantly impact the blue response. If placed on a non-illuminated side, the skin's parasitic absorption leads to a reduced red response. This internal skin parasitic absorption is the focus of this work.

As the NIR parasitic absorption cannot be directly separated from the active generation A_{gen} from purely optical measurements, optical modeling is essential for the quantification. Ray tracing in combination with wave-optics modeling within the near-surfaces (e.g. transfer-matrix-method TMM) is in principle well suitable for this task, which however requires detailed knowledge of the cell's and all optical layer's properties. The high number of input parameters, and the often substantial uncertainties mainly in refractive index data, result in substantial effort to properly calibrate the ray tracing model to experimental measurements. A simpler modeling approach was introduced by Basore [11] in PC1D [12,13], which we call the "Basore model". It essentially requires the external transmission T_{ext} as a spectral input parameter, which can be deduced from reflectance measurements, and then analytically models light-trapping by internal optical properties of the skins, mainly the skin's internal reflection. The Basore model has been widely applied, not only via its implementation in PC1D, and thereby proven highly useful for an electro-optical analysis of silicon solar cells [14–18]. The low number of input parameters as well as the rapid analytical calculations makes its application much simpler and faster compared to ray tracing. In particular, it enables rapid and highly automatable calibration of the input parameters by fitting them to measured reflectance, absorptance and transmittance (RAT) measurements, to accurately discriminate the generation from various optical losses [19].

This work extends the Basore model by introducing an additional input parameter representing the parasitic absorption in a skin, namely the absorbed fraction per perpendicular pass A_{ppp}. Generally, A_{ppp} is agnostic about the nature of the parasitic absorption, i.e. the properties of the materials involved and the detailed optical effects leading to such parasitic absorption. But it is emphasized that the scope is on light-trapping, meaning that other relevant optical properties of the skin, namely the reflection and first-pass absorption for a skin on the illuminated side, are not addressed by A_{ppp}. Those effects are rather inputs into the proposed model, which can often be directly deduced from measurements. We investigate and validate the physical meaningfulness of this parameter by investigating various experimental samples and solar cells.

2. Model description

The Basore model is typically used to quantify the individual contributions influencing a spectral response (SR) measurement, an example being shown in Fig. 1. The principle of the model is to analytically trace a representative ray as sketched in Fig. 2. The inputs into the original Basore model are the following: the *external* optics is fully defined by the external transmission T_{ext}, which is the fraction of incident photons reaching the actively absorbing bulk, i.e. neither reflected nor parasitically absorbed in the skin during the first pass. T_{ext} can be deduced from the measured reflectance R by extrapolation in the long wavelength region to discriminate escape reflectance R_{esc} and the external reflectance R_{ext}, and subtracting the absorption in the skin during the first pass A_{ext}: $T_{ext} = 1 - R_{ext} - A_{ext}$. The *internal* optics, i.e. light-trapping, is defined by the internal reflection parameters at the front and back side for the first and nth pass R_{f1}, R_{fn}, R_{b1} and R_{bn}, which are approximated to be wavelength-independent. Additional inputs are a representative facet angle in case of a textured surface, as well as an option on each side to define whether reflections are specular or diffuse.

The model can predict the spectral escape reflectance R_{esc}, transmittance T, absorptance A, as well as the depth-resolved generation profile [15,21,22]. Its implementation in PC1D already considers parasitic absorption in the absorber via FCA depending on the defined spatially resolved doping density [18] to differentiate the parasitic FCA absorptance $A_{FCA,bulk}$ from the band-to-band absorptance A_{gen} contributing to the generated current density.

Here, we introduce an additional lumped internal optical input parameter to account for parasitic absorption specifically in the skin: the absorbed fraction per perpendicular pass, A_{ppp}, on the front and back side, respectively. The model then accounts for the multiple passes with the angles θ_1, θ_0 and θ_n through this absorptive layer. For each internal reflection the intensity of the representative ray is not only reduced by 1-R_x, but by $A_{ppp} \cos\theta_x (1 - R_x) A_{ppp} \cos\theta_x$, where x denotes the corresponding index for the first or nth pass at the front or rear side. The main additional output of the extended Basore model is then the spectrally

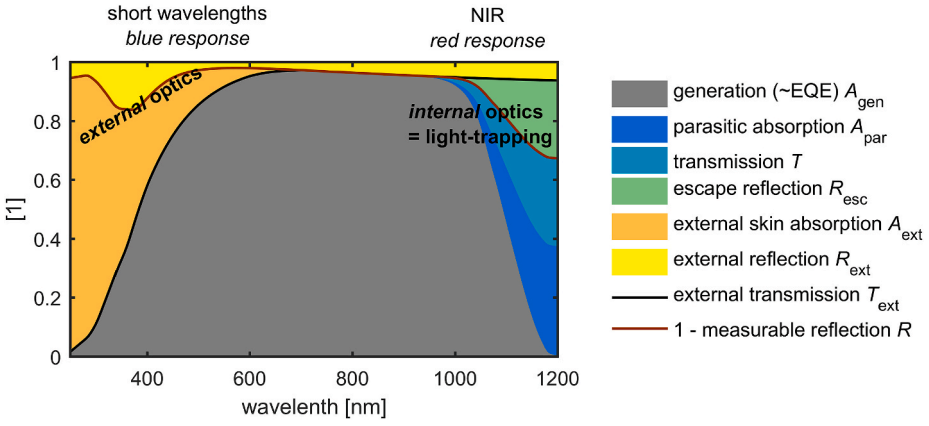

Fig. 1. Overview of an exemplary spectral response for a Fraunhofer ISE SHJ solar cell investigated in section 3.3 (a cell with higher than usual parasitic absorption), highlighting the terminology used throughout this work; the black line divides *external* optics (= external transmission T_{ext}) and *internal* optics (= light-trapping).

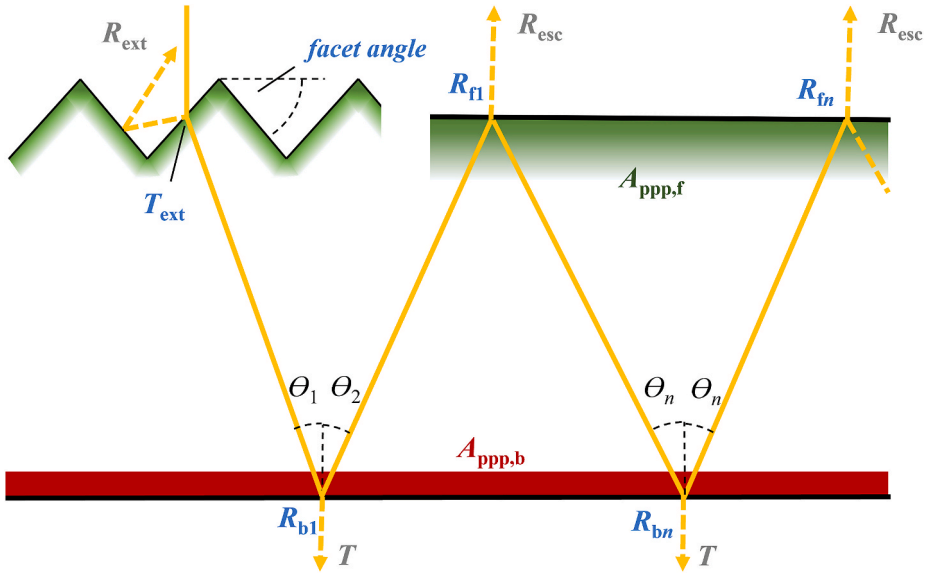

Fig. 2. Sketch of the light-trapping model introduced by Basore [20] (input parameters in *blue*), including this work's extension by an additional input parameter A_{ppp} on each side to account for the respective skin's parasitic absorption; the exemplary cell design features a boron doping profile at the textured front, and an n-type poly-silicon layer at the planar back. (For interpretation of the references to colour in this figure legend, the reader is referred to the Web version of this article.)

resolved total parasitic skin absorption on the front and rear side resulting from multiple passes through A_{ppp}, and a decreased active absorption A_{gen}.

Two useful approaches to define A_{ppp} either as a wavelength-dependent or single-valued quantity can be distinguished:

i) calculating A_{ppp} as a *wavelength-dependent quantity* from the optical properties of the skin, e.g. for the following two cases: for FCA within a known near-surface doping profile, A_{ppp} is found by numerical integration over the profile using the FCA parameterization in Ref. [8]; for a doped poly-Si layer, if the same optical properties as for c-Si can be assumed [23], A_{ppp} can be calculated via the Lambert-Beer law using the sum of the FCA [8] and band-to-band absorption coefficient [24] α and the layer thickness t: $A_{ppp} = 1 - e^{\alpha t}$, which notably assumes zero collection of generated carriers; see Fig. 3 for exemplary wavelength-dependent values of A_{ppp};
ii) assuming a *constant single value* for A_{ppp}, which is useful for analyzing a sample with an absorbing layer with unknown properties; the constant assumption is not detrimental, as the wavelength range relevant for light-trapping is relatively narrow, see Fig. 3.

Care must be taken if a non-zero A_{ppp} is defined on an illuminated side: if the wavelength-dependence of A_{ppp} is known, e.g. by calculating it in approach i), it can be useful to apply A_{ppp} to also quantify the first-pass external absorption losses for all wavelengths, in which case A_{ppp} also represents losses normally contained in A_{ext}. E.g. when a bifacial cell with a rear poly-Si layer is illuminated from the rear side, A_{ppp} can represent both the strong blue response losses due to band-band-absorption, as well as the NIR light trapping losses. However, if A_{ppp} is assumed a constant single value, the value is usually valid in the light-trapping regime only (see Fig. 3), and is therefore highly inaccurate in quantifying the short-wavelength absorption losses during the first pass. In this case A_{ppp} can not be applied to the first pass, but the first pass skin absorption losses must be separately accounted for in A_{ext} even if they originate from the same physical absorption mechanism in the same material layer. See e.g. section 3.3 for this scenario.

Consequently, when using A_{ppp} as a single value, it must be kept in mind that this value is applicable for the NIR light-trapping losses only, and does not fully define the "transparency" of the skin.

The spectral model results can be integrated with the AM1.5 g spectrum to yield a breakdown of the generation current density and light trapping loss components: escape reflection, transmission and parasitic absorption in the bulk as well in the front and rear skins. Due to the simplicity of the inputs and the rapid calculation of this analytical model, a particular useful application is the fitting to RAT measurements to calibrate the optical properties of a particular experimental sample or solar cell. This has been shown to work well, as judged by an accurate prediction of A_{gen}, in particular if employing the simplification of equal first and nth pass reflections ($R_f = R_{f1} = R_{fn}$ and $R_b = R_{b1} = R_{bn}$) to reduce the number of fit parameters and thus to avoid overfitting [19]. For all modeling in this work we use the solar cell simulator Quokka 3 [7], which implements the extended Basore model as well as a non-linear-least-squares curve-fitting functionality.

3. Application examples

3.1. Free carrier absorption in diffused doping profiles

Here we investigate the suitability of the extended Basore model to quantify FCA losses in doping profiles. For this we use the experimental data by Rüdiger et al. [6], where reflectance was measured on front-side textured, back-side planarized and metallized samples with various doping profiles either at the front, back or both sides. Notably, the reflectance was very similar comparing front (textured) and back (planarized) diffused samples, indicating that FCA at a textured surface can well be modelled in a planar modeling domain, as assumed in the extended Basore model. We fit the Basore model to the reference sample without any diffusion, which gives a very good match with an coefficient of determination $R^2 = 99.98\%$ between 800 and 1200 nm. Next, we model the reflectance by including a wavelength-dependent A_{ppp} calculated from the respective doping profiles. Fig. 4 shows that this work's model agrees to the experimental data similarly well as compared to Ref. [6]. We conclude that the extended Basore model provides a useful accuracy to quantify FCA in doped Si layers, both on textured and planarized surfaces. Notably, the escape reflectance is overestimated by $\geq 10\%_{rel}$ when using the FCA parameterization of Rüdiger [6], meaning that the parameterization of Baker-Finch [8] is found more accurate in this work's model. An overview of the resulting

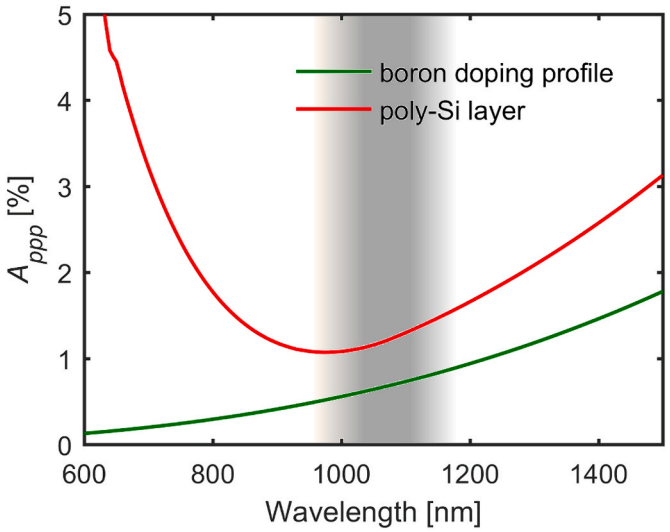

Fig. 3. Exemplary wavelength-dependence of A_{ppp} for a boron doping profile (*green*) resulting from free-carrier absorption, and for an n-type poly-Si layer (*red*) resulting from both free-carrier and band-to-band absorption; the grey area indicates the wavelength range relevant for light-trapping. (For interpretation of the references to colour in this figure legend, the reader is referred to the Web version of this article.)

A_{ppp} values is given in Table 2.

3.2. Free carrier absorption in poly-silicon layer of TOPCon solar cells

Here we analyze TOPCon solar cells with the only controlled variation being the thickness and doping concentration of the back side poly-Si layer, as published in Ref. [23], similar to the approach presented in Ref. [14]. The batch includes a reference cell with a very thin TOPCon layer and consequently negligible parasitic absorption. Both reflectance R and external quantum efficiency (EQE) are measured. Due to the cells being electrically very good, the influence of carrier collection loss on EQE is negligible, and therefore EQE can be assumed to equal A_{gen}. For each solar cell with an absorbing poly-Si layer the J_{sc} loss ΔJ_{sc} is then calculated via integrating the difference to the reference cell's EQE over the AM1.5 g spectrum between 950 nm and 1200 nm. Notably, besides the expected reduction in escape reflectance, the cells also differ in external reflection, resulting in J_{sc} differences not related to parasitic absorption with a similar magnitude. We attempt to minimize this artifact by normalizing the EQE at 900 nm, however one can still expect some significant error on the results.

In a first *predictive* modeling approach, we only fit the Basore model once to the reflectance of the reference cell. We calculate the back side A_{ppp} from the poly-Si properties, which were independently measured on test structures, and insert the resulting value in the previously calibrated model for the reference cell. This way the influence of the poly-Si layer with known properties on escape reflection and A_{gen} is predicted.

In a second *fit* approach, we disregard the knowledge of the poly-Si layer properties and individually fit the extended Basore model to each cell's reflectance using A_{ppp} as a fit parameter, while keeping the rear internal reflection at the fit result from the reference cell.

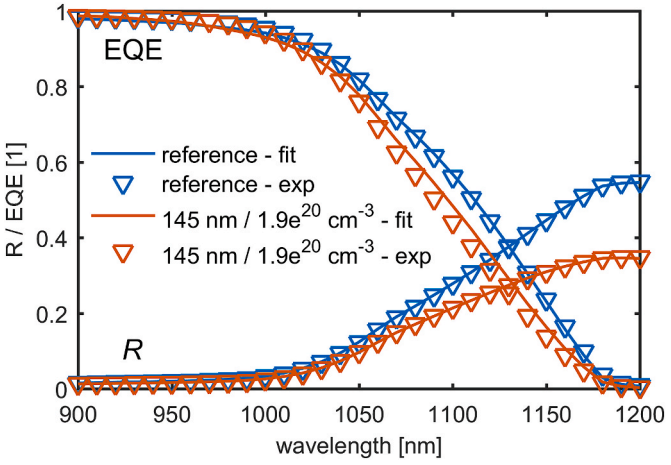

Fig. 5. Reflectance R and external quantum efficiency EQE for the reference and the heaviest doped poly-Si layer TOPCon cell, comparing measurements (*symbols*) and calculations using this work's model (*lines*).

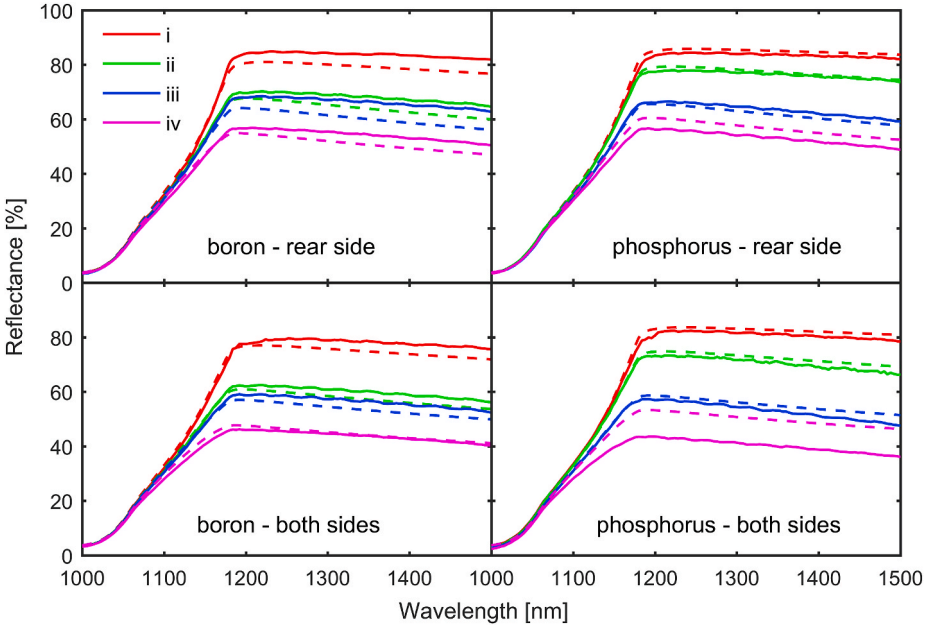

Fig. 4. Comparison of measured (solid lines [6]) and modelled (dashed lines) reflection spectra using the model of this work and A_{ppp} calculated from the doping profiles i to iv; equivalent to Fig. 5 of Ref. [6].

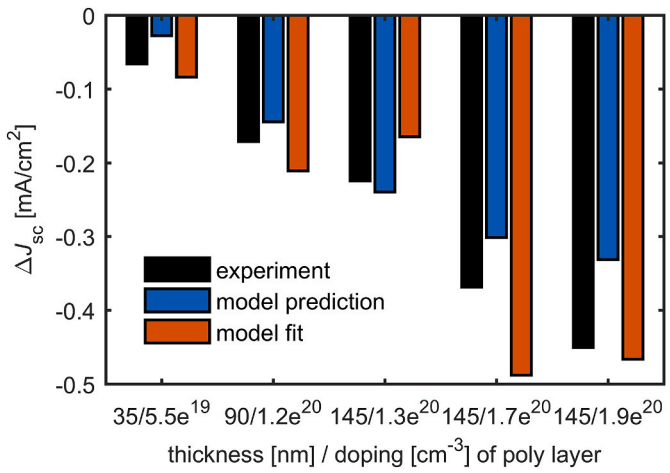

Fig. 6. J_{sc} loss of TOPCon solar cells with varying poly-Si properties relative to the reference cell, experimental data from Ref. [23]; *model prediction*: using the independently measured poly-Si properties to calculate A_{ppp}; *model fit*: fitting the extended Basore model with a single-valued A_{ppp} to the reflectance individually.

The satisfactory agreement in Fig. 6 means that the J_{sc} loss due to parasitic absorption in a poly-Si layer can be estimated with useful accuracy both predictively as well as by fitting using this work's model. As mentioned above, due to the cell-to-cell variations, it is not possible to tell whether the experimental, predicted or fitted J_{sc} loss is closest to reality, but the deviations are likely within the experimental uncertainty. An overview of the A_{ppp} values comparing predicted and fitted ones is given in Table 2.

3.3. Parasitic absorption in a-Si and TCO layers of HJT solar cell

Here we analyze a both-sides textured bifacial silicon heterojunction (SHJ) solar cell manufactured at Fraunhofer ISE [25]. As typical for SHJ cells, an optical loss is the parasitic absorption in the skin on both sides, namely in the amorphous silicon (a-Si) and transparent conductive oxide (TCO) layers. In this example we show how these losses can be quantified without knowledge of the layer's optical properties, by using a wavelength-independent A_{ppp} on each side as fit parameters.

Reflectance R and EQE is measured for front and rear illumination, and equivalent to the TOPCon cells in the previous section EQE $\approx A_{gen}$ can be assumed. As the measurements were performed on the cell including the metal grid, we first correct for metal reflection by shifting the reflectance so that the minimum value equals zero. Next, the external absorption losses A_{ext} on each side are calculated by $A_{ext} = 1 - R_{ext}$ − EQE up to ~800 nm, and then assumed constant in the long wavelength regime. This neglects some expected increase towards higher wavelengths due to increasing FCA. However, this assumption is deemed not detrimental due to the low value of A_{ext}, and cannot be otherwise determined more accurately solely from the RAT measurements. See Fig. 7 for an overview of the spectral quantities.

What cannot be directly deduced from the measurements are the parasitic absorption losses in the NIR, which are also caused by parasitic absorption in the a-Si and TCO layers, but are now separately defined via A_{ppp} in order for their determination. In this case there is no sufficient knowledge of the optical properties of these absorbing layers, that's why we choose to fit a single-valued A_{ppp} on each side. The extended Basore model is then fitted simultaneously to the measured front and rear illuminated reflectance with initially four fit parameters: a single internal reflection and A_{ppp} on each side. The resulting parameter values including the 95% confidence bounds are shown in Table 1. We first note that the internal reflection values are very close to the Lambertian limit of $1 - \frac{1}{n^2} \approx 0.92$. This is reasonable as both sides are textured and gives evidence that the calibrated model is a physically sound representation of the cell's optics. Furthermore, the calibrated model predicts the EQE in the light-trapping regime very accurately, both for front and rear illumination with a single set of input parameters, see Fig. 7, confirming the model's power in predicting generation from a reflection fit. However, we also observe a substantial error of A_{ppp} on each side, which we find to be a covariance error. By performing a second fit with only three fit parameters, via forcing A_{ppp} to be equal on both sides, the error becomes low. This means that the total losses arising from A_{ppp} on both sides are accurate, but the discrimination between front and back side A_{ppp} cannot be done with useful confidence. This is reasonable as both A_{ppp} values are expected to have a very similar influence on the NIR reflectance.

Fig. 8 shows the resulting AM1.5 g current density loss breakdown for the calibrated model. Notably, the loss breakdown is achieved via reflectance and EQE measurements requiring only minimal information about the cell's properties, namely the thickness and that both sides are textured.

Table 1
Fit parameter results from fitting the extended Basore model to front and rear reflectance of the investigated SHJ solar cell, including the 95% confidence bounds.

parameter	4 parameter fit	3 parameter fit ($A_{ppp,f} = A_{ppp,b}$)
$R_f = R_{f1} = R_{fn}$	90.6 ± 2.5%	91.8 ± 0.1%
$R_b = R_{b1} = R_{bn}$	91.2 ± 2.4%	91.9 ± 0.2%
$A_{ppp,f}$	0.1 (lower bound) ± 15.6%	1.41 ± 0.03%
$A_{ppp,b}$	3.1 ± 15.1%	

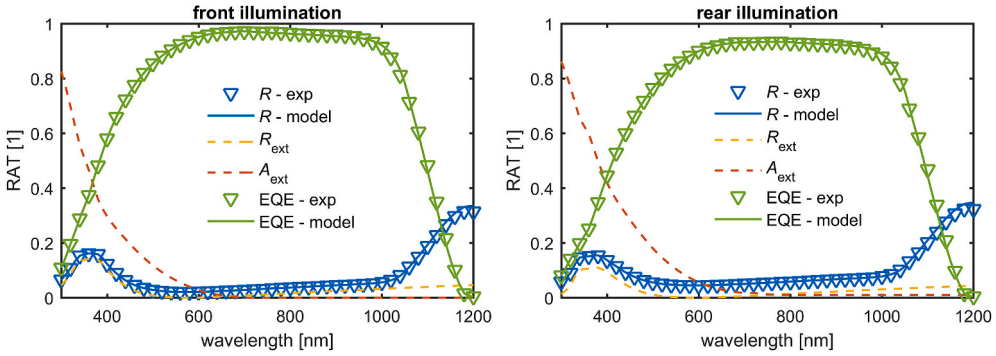

Fig. 7. Spectral properties of the investigated SHJ for front and rear illumination, comparing measurements (*symbols*) with this work's modeling (*lines*); the extended Basore model was fitted to front and rear reflectance simultaneously, accurately predicting the band-to-band absorptance (=EQE).

Table 2
Overview of A_{ppp} values determined in this work, either explicitly calculated or fitted to RAT measurements; the deviation between calculated and fitted values for the poly-Si layer is to a large part explainable by cell-to-cell differences not related to the poly-Si layer, but the magnitude and trend is still comparable.

description	A_{ppp} calculated@ 1100 nm	single-valued A_{ppp} fitted to RAT
doping profiles from Ref. [6] (sheet resistance)		
boron profile i) (188 Ω/sq)	0.13%	
boron profile ii) (89 Ω/sq)	0.47%	
boron profile iii) (89 Ω/sq)	0.62%	
boron profile iv) (42 Ω/sq)	1.1%	
phosphorus profile i) (421 Ω/sq)	0.09%	
phosphorus profile ii) (182 Ω/sq)	0.26%	
phosphorus profile iii) (75 Ω/sq)	0.85%	
phosphorus profile iv) (54 Ω/sq)	1.2%	
n-type poly-Si layer from Ref. [23] (thickness/doping density)		
i) (35 nm/5.5•10^{19} cm^{-3})	0.13%	0.57%
ii) (90 nm/1.2•10^{20} cm^{-3})	0.72%	1.14%
iii) (145 nm/1.3•10^{20} cm^{-3})	1.3%	1.0%
vi) (145 nm/1.7•10^{20} cm^{-3})	1.6%	2.3%
v) (145 nm/1.9•10^{20} cm^{-3})	1.8%	2.5%
SHJ a-Si + TCO stack from [23]		
average value for front and rear side		1.4%

4. A third figure of merit for a passivating contact

The electrical quality of a passivating contact is typically given by two figures of merit, namely the recombination parameter J_{0c} and the contact resistivity ρ_c. While neglecting some possible non-idealities of real passivating contacts, those two single-valued quantities have been very successful in judging and comparing the quality of passivating contacts, see e.g. Ref. [1].

While it is well known that the optical properties are equally detrimental due to the often substantial parasitic absorption, no such optical figure of merit has been established yet. We thus suggest A_{ppp} as a third single-valued figure of merit judging the optical losses due to parasitic absorption within a solar cell. However, as discussed above, it is important to be aware that a single-valued A_{ppp} is valid only in the NIR and is not applicable to quantify the blue response losses, i.e. the full spectral transparency of a passivating contact. A_{ppp} as a figure of merit is therefore specifically useful for the case of a passivating contact being employed on a non-illuminated side, i.e. on the back side.

The values for A_{ppp} determined in this work are summarized in Table 2 to give an impression of the magnitude of this quantity. Furthermore, to illustrate the impact of A_{ppp} on solar cell performance, we perform 1D simulations of an Auger-limited solar cell with ideal monofacial and bifacial optical properties, and vary the back side A_{ppp}. The cell thickness is set to a typical value of 150 µm, intrinsic recombination is modelled as in Ref. [26], and very small bulk doping is assumed. Ideal unity external front side transmission is assumed, and the internal reflections are set to the Lambertian limit of $1 - \frac{1}{n^2}$, except for the monofacial cell's back side which is set to 100%. Fig. 9 reveals an efficiency loss for $A_{ppp} = 1\%$ of a few 0.1 $\%_{abs}$, which will be somewhat lower for a realistic solar cell. This means that as a rule of thumb, A_{ppp} should be aimed below 1% to ensure no significant current and efficiency loss within a silicon solar cell. Notably, this threshold applies to the case of a full-area passivating contact. For a localized passivating contact, this threshold is approximately increased by the inverse of the contact fraction.

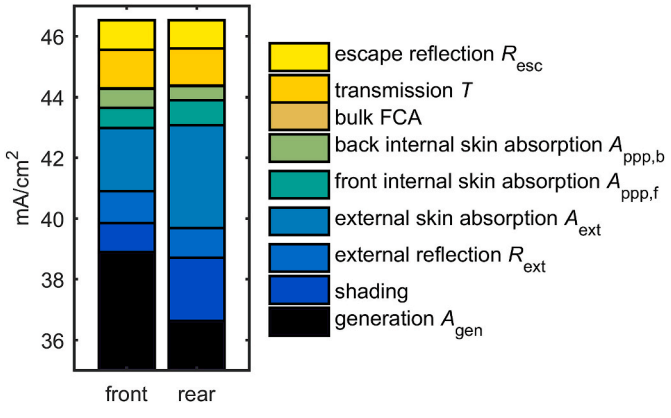

Fig. 8. Current density losses of the SHJ solar cell as determined by the extended Basore model, calibrated to measured front and rear reflectance; the parasitic absorption in the a-Si and TCO layers appears as both, external (during first pass on illuminated side) A_{ext} and internal (subsequent passes) A_{ppp} skin absorption losses.

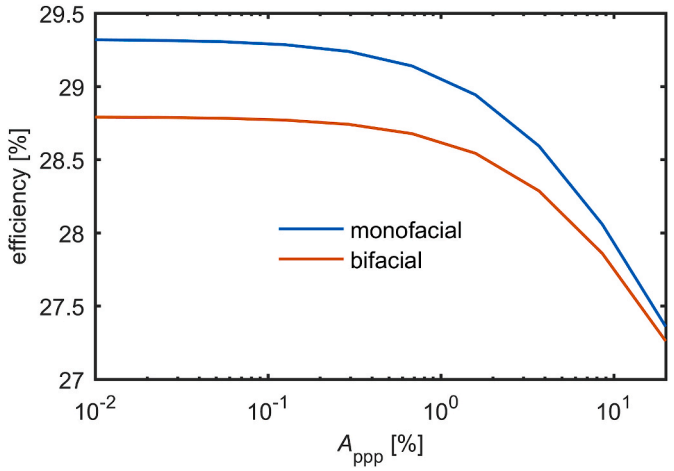

Fig. 9. Efficiency of a one-dimensional 150 µm thick ideal solar, with intrinsic recombination only and ideal Lambertian optics, as a function of the back side parasitic absorption parameter A_{ppp}.

5. Conclusions

In this work we extended the analytical light-trapping model by Basore to account for parasitic absorption in the skins via the lumped parasitic absorption parameter A_{ppp}, specifically for the near-infrared (NIR)/red response of a solar cell. As the original model, the model of this work is applicable to wafer-based Si solar cells. The model can well be calibrated by fitting the input parameters, including a single-valued A_{ppp} to reflectance measurements of a sample or solar cell, not requiring any detailed information of its optical properties other than the thickness and whether the surfaces are textured or planar. Such a calibrated model can predict the influence of parasitic absorption on the light-trapping performance as well as a current loss breakdown under AM1.5 g illumination with useful accuracy, as shown for TOPCon solar cells and a SHJ solar cell. We also show for two cases how A_{ppp} can be calculated as a function of wavelength: i) FCA in c-Si doping profiles, and ii) total absorption in a poly-Si layer assumed to have the same optical properties as c-Si. In both cases the influence on NIR parasitic absorption is again predicted with useful accuracy.

Having proven the usefulness of A_{ppp} to represent light-trapping losses as a single-valued quantity, we suggest A_{ppp} as a third figure of merit for the quality of a passivating contact, next to the recombination parameter J_{0c} and the contact resistivity ρ_c. Via idealized solar cell simulations assuming a full-area back side skin with parasitic absorption, we determine a rule-of-thumb threshold for A_{ppp} of approx. 1%, below which parasitic absorption has no significant impact on generated current density and thus efficiency.

Declaration of competing interest

The authors declare that they have no known competing financial interests or personal relationships that could have appeared to influence the work reported in this paper.

Acknowledgements

This work was financially supported by the German Federal Ministry for Economic Affairs and Energy and by industry partners within the research project “GENESIS” under grant number 0324274C.

References

[1] T.G. Allen, J. Bullock, X. Yang, A. Javey, S. de Wolf, “Passivating contacts for crystalline silicon solar cells,” (in En;en), Nat Energy 4 (11) (2019) 914–928, https://doi.org/10.1038/s41560-019-0463-6.

[2] C. Messmer, A. Fell, F. Feldmann, N. Wohrle, J. Schon, M. Hermle, Efficiency roadmap for evolutionary upgrades of PERC solar cells by TOPCon: impact of parasitic absorption, IEEE J. Photovoltaics 10 (2) (2020) 335–342, https://doi.org/10.1109/JPHOTOV.2019.2957642.

[3] Z.C. Holman, et al., Infrared light management in high-efficiency silicon heterojunction and rear-passivated solar cells, J. Appl. Phys. 113 (1) (2013), https://doi.org/10.1063/1.4772975.

[4] M. Balestrieri, D. Pysch, J.-P. Becker, M. Hermle, W. Warta, S.W. Glunz, Characterization and optimization of indium tin oxide films for heterojunction solar cells, Sol. Energy Mater. Sol. Cell. 95 (8) (2011) 2390–2399, https://doi.org/10.1016/j.solmat.2011.04.012.

[5] P. Procel, et al., Opto-electrical modelling and optimization study of a novel IBC c-Si solar cell, Prog. Photovoltaics Res. Appl. 25 (6) (2017) 452–469, https://doi.org/10.1002/pip.2874.

[6] M. Ruediger, J. Greulich, A. Richter, M. Hermle, Parameterization of free carrier absorption in highly doped silicon for solar cells, IEEE Trans. Electron. Dev. 60 (7) (2013) 2156–2163, https://doi.org/10.1109/TED.2013.2262526.

[7] A. Fell, J. Schön, M.C. Schubert, S.W. Glunz, The concept of skins for silicon solar cell modeling, Sol. Energy Mater. Sol. Cell. 173 (Supplement C) (2017) 128–133, https://doi.org/10.1016/j.solmat.2017.05.012.

[8] S.C. Baker-Finch, K.R. McIntosh, Di Yan, K.C. Fong, T.C. Kho, Near-infrared free carrier absorption in heavily doped silicon, J. Appl. Phys. 116 (6) (2014), https://doi.org/10.1063/1.4893176.

[9] F. Feldmann, M. Bivour, C. Reichel, M. Hermle, S.W. Glunz, Passivated rear contacts for high-efficiency n-type Si solar cells providing high interface passivation quality and excellent transport characteristics, Sol. Energy Mater. Sol. Cell. 120 (2014) 270–274.

[10] Z.C. Holman, et al., Current losses at the front of silicon heterojunction solar cells, IEEE J. Photovoltaics 2 (1) (2012) 7–15, https://doi.org/10.1109/JPHOTOV.2011.2174967.

[11] P.A. Basore, Numerical modeling of textured silicon solar cells using PC-1D, IEEE Trans. Electron. Dev. 37 (2) (1990) 337–343, https://doi.org/10.1109/16.46362.

[12] H. Haug, J. Greulich, PC1Dmod 6.2 – improved simulation of c-Si devices with updates on device physics and user interface, Energy Procedia 92 (2016) 60–68, https://doi.org/10.1016/j.egypro.2016.07.010.

[13] D.A. Clugston, P.A. Basore, PC1D version 5: 32-bit solar cell modeling on personal computers, in: 26th Photovoltaic Specialists Conference, 1997, pp. 207–210.

[14] M. Fırat, M.R. Payo, F. Duerinckx, J.-M. Luchies, M. Lenes, J. Poortmans, Characterization of absorption losses in rear side n-type polycrystalline silicon passivating contacts, in: 15th International Conference on Concentrator Photovoltaic Systems (CPV-15), Fes, Morocco, 2019, p. 40004.

[15] R. Brendel, M. Hirsch, R. Plieninger, J.J.H. Werner, Quantum efficiency analysis of thin-layer silicon solar cells with back surface fields and optical confinement, IEEE Trans. Electron. Dev. 43 (7) (1996) 1104–1113.

[16] D. Kray, M. Hermle, S.W. Glunz, Theory and experiments on the back side reflectance of silicon wafer solar cells, Prog. Photovoltaics Res. Appl. 16 (1) (2008) 1–15, https://doi.org/10.1002/pip.769.

[17] C. Schinke, D. Hinken, J. Schmidt, K. Bothe, R. Brendel, Modeling the spectral luminescence emission of silicon solar cells and wafers, IEEE J. Photovoltaics 3 (3) (2013) 1038–1052, https://doi.org/10.1109/jphotov.2013.2263985.

[18] D.A. Clugston, P.A. Basore, Modelling free-carrier absorption in solar cells, Prog. Photovoltaics Res. Appl. 5 (4) (1997) 229–236, https://doi.org/10.1002/(SICI)1099-159X(199707/08)5:4<229::AID-PIP164>3.0.CO;2-6.

[19] A. Fell, W. Wirtz, H. Höffler, J. Greulich, Determining the generation rate of silicon solar cells from reflection and transmission measurements by fitting an analytical optical model, in: 2019 IEEE 46th Photovoltaic Specialists Conference, PVSC), Chicago, IL, USA, 2019, pp. 3037–3041.

[20] J.A. Rand, P.A. Basore, “Light-trapping Silicon Solar Cells-Experimental Results and Analysis,” in *22nd Photovoltaic Specialists Conference*, Las Vegas, 1991, pp. 192–197.

[21] A. Fell, K.R. McIntosh, K.C. Fong, Simplified device simulation of silicon solar cells using a lumped parameter optical model, IEEE J. Photovoltaics (2016) 1–6, https://doi.org/10.1109/JPHOTOV.2016.2528407.

[22] S.C. Baker-Finch, K.R. McIntosh, One-dimensional photogeneration profiles in silicon solar cells with pyramidal texture, Prog. Photovoltaics Res. Appl. 20 (1) (2012) 51–61, https://doi.org/10.1002/pip.1109.

[23] F. Feldmann, M. Nicolai, R. Müller, C. Reichel, M. Hermle, Optical and electrical characterization of poly-Si/SiOx contacts and their implications on solar cell design, Energy Procedia 124 (2017) 31–37, https://doi.org/10.1016/j.egypro.2017.09.336.

[24] C. Schinke, K. Bothe, P.C. Peest, J. Schmidt, R. Brendel, Uncertainty of the coefficient of band-to-band absorption of crystalline silicon at near-infrared wavelengths, Appl. Phys. Lett. 104 (8) (2014) 81915.

[25] A. Moldovan, et al., “Improved Layer Properties Combined with Light Soaking Enabling for 23% Efficient Silicon Heterojuction Solar Cells,” *37th European Photovoltaic Solar Energy Conference And Exhibition*, 2020, pp. 218–222, https://doi.org/10.4229/EUPVSEC20202020-2BO.5.2.

[26] A. Richter, S.W. Glunz, F. Werner, J. Schmidt, A. Cuevas, Improved quantitative description of Auger recombination in crystalline silicon, Phys. Rev. B 86 (16) (2012) 165202.